

Persistent Quantum Beats and Long-Distance Entanglement from Waveguide-Mediated Interactions

Huaixiu Zheng* and Harold U. Baranger†

Department of Physics, Duke University, P.O. Box 90305, Durham, North Carolina 27708, USA

(Dated: Phys. Rev. Lett. **110**, 113601 (2013); March 12, 2013)

We study photon-photon correlations and entanglement generation in a one-dimensional waveguide coupled to two qubits with an arbitrary spatial separation. To treat the combination of nonlinear elements and 1D continuum, we develop a novel Green function method. The vacuum-mediated qubit-qubit interactions cause quantum beats to appear in the second-order correlation function. We go beyond the Markovian regime and observe that such quantum beats persist much longer than the qubit life time. A high degree of long-distance entanglement can be generated, increasing the potential of waveguide-QED systems for scalable quantum networking.

PACS numbers: 42.50.Ex, 03.67.Bg, 42.50.Ct, 42.79.Gn

One-dimensional (1D) waveguide-QED systems are emerging as promising candidates for quantum information processing [1–14], motivated by tremendous experimental progress in a wide variety of systems [15–24]. Over the past few years, a *single* emitter strongly coupled to a 1D waveguide has been studied extensively [2–8, 10, 12–14]. To enable greater quantum networking potential using waveguide-QED [1], it is important to study systems having more than just one qubit.

In this Letter, we study cooperative effects of *two* qubits strongly coupled to a 1D waveguide, finding the photon-photon correlations and qubit entanglement beyond the well-studied Markovian regime [25–28]. A key feature is the combination of these two highly nonlinear quantum elements with the 1D continuum of states. In comparison to either linear elements coupled to a waveguide [29–32] or two qubits coupled to a single mode serving as a bus [33], both of which have been studied previously, new physical effects appear. To study these ef-

fects, we develop a numerical Green function method to compute the photon correlation function for an arbitrary interqubit separation.

The strong quantum interference in 1D, in contrast to the three-dimensional case [34], makes the vacuum-mediated qubit-qubit interaction [35] long-ranged. We find that quantum beats emerge in the photon-photon correlations, and persist to much longer time scales in the non-Markovian regime. We show that such persistent quantum beats arise from quantum interference between emission from two subradiant states. Furthermore, we demonstrate that a high-degree of long-distance entanglement can be generated, thus supporting waveguide-QED-based open quantum networks.

Hamiltonian.—As shown in Fig. 1(a), we consider two qubits with transition frequencies ω_1 and ω_2 , separation $L = \ell_2 - \ell_1$, and dipole couplings to a 1D waveguide. The Hamiltonian of the system is [36]

$$H = \sum_{j=1,2} \hbar(\omega_j - i\Gamma'_j/2)\sigma_j^+\sigma_j^- + H_{wg} + \sum_{j=1,2} \sum_{\alpha=R,L} \int dx \hbar V_j \delta(x - \ell_j) [a_\alpha^\dagger(x)\sigma_j^- + \text{h.c.}],$$

$$H_{wg} = \int dx \frac{\hbar c}{i} \left[a_R^\dagger(x) \frac{d}{dx} a_R(x) - a_L^\dagger(x) \frac{d}{dx} a_L(x) \right], \quad (1)$$

where $a_{R,L}^\dagger(x)$ is the creation operator for a right- or left-going photon at position x and c is the group velocity of photons. σ_j^+ and σ_j^- are the qubit raising and lowering operators, respectively. An imaginary term in the energy level is included to model the spontaneous emission of the excited states at rate $\Gamma'_{1,2}$ to modes other than the waveguide continuum [37]. The decay rate to the waveguide continuum is given by $\Gamma_j = 2V_j^2/c$. Throughout the Letter, we assume two identical qubits: $\Gamma_1 = \Gamma_2 \equiv \Gamma$, $\omega_1 = \omega_2 \equiv \omega_0 \gg \Gamma$, and $\Gamma'_1 = \Gamma'_2 \equiv \Gamma'$.

Single-photon phase gate.— Assuming an incident photon from the left (with wave vector k), we obtain the single photon scattering eigenstate [38]; the transmission

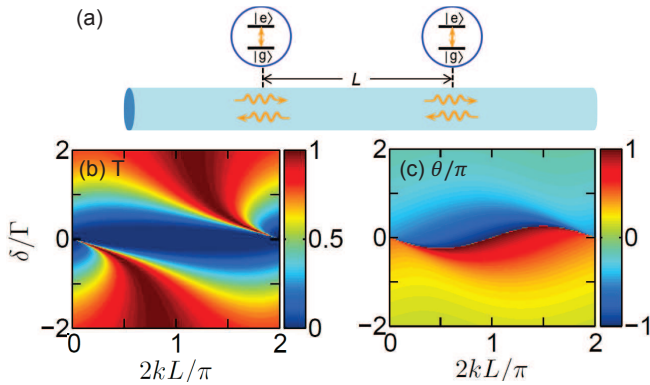


FIG. 1. Schematic diagram of the waveguide system and single-photon transmission. (a) Two qubits (separated by L) interacting with the waveguide continuum. Panels (b) and (c) show colormaps of the single-photon transmission probability T and the phase shift θ , respectively, as a function of detuning $\delta = ck - \omega_0$ and $2kL$. Here, we consider the lossless case $\Gamma' = 0$.

coefficient is given by

$$t_k \equiv \sqrt{T}e^{i\theta} = \frac{(ck - \omega_0 + \frac{i\Gamma'}{2})^2}{(ck - \omega_0 + \frac{i\Gamma + i\Gamma'}{2})^2 + \frac{\Gamma^2}{4}e^{2ikL}}. \quad (2)$$

As shown in Fig. 1(b), there is a large window of perfect transmission: $T \approx 1$, even when the detuning ($\delta = ck - \omega_0$) of the single photon is within the resonance line width ($\sim \Gamma$). This is in sharp contrast to the single-qubit case, where perfect transmission is only possible for far off-resonance photons [3]. Such perfect transmission occurs when the reflections from the two qubits interfere destructively and cancel each other completely. Furthermore, Fig. 1(c) shows that within the resonance line width, there is a considerable phase shift θ . This feature of single-photon transmission can be used to implement a photon-atom phase gate. For example, in the case of $\delta = -0.5\Gamma$ and $kL = \pi/4$, the single photon passes through the system with unit probability and a $\pi/2$ phase shift. Two successive passes will give rise to a photon-atom π -phase gate, which can be further used to realize a photon-photon phase gate [39].

Photon-photon correlation: Nonlinear effects.—To study the interaction effects, we develop a novel Green function method to calculate the full interacting scattering eigenstates and so photon-photon correlations. We start with a reformulated Hamiltonian [6]

$$\begin{aligned} H &= H_0 + V, \quad V = \sum_{j=1,2} \frac{U}{2} d_j^\dagger d_j (d_j^\dagger d_j - 1), \\ H_0 &= \sum_{j=1,2} \hbar(\omega_j - i\Gamma'_j/2) d_j^\dagger d_j + H_{wg} \\ &+ \sum_{j=1,2} \sum_{\alpha=R,L} \int dx \hbar V_j \delta(x - a_j) [a_\alpha^\dagger(x) d_j + \text{h.c.}], \end{aligned} \quad (3)$$

where d_j^\dagger and d_j are bosonic creation and annihilation operators on the qubit sites. The qubit ground and excited states correspond to zero- and one-boson states, respectively. Unphysical multiple occupation is removed by including a large repulsive on-site interaction term U ; the Hamiltonians in Eqs. (1) and (3) become equivalent in the limit $U \rightarrow \infty$. The non-interacting scattering eigenstates can be obtained easily from $H_0|\phi\rangle = E|\phi\rangle$. The full interacting scattering eigenstates $|\psi\rangle$ are connected to $|\phi\rangle$ through the Lippmann-Schwinger equation [11, 40, 41]

$$|\psi\rangle = |\phi\rangle + G^R(E)V|\psi\rangle, \quad G^R(E) = \frac{1}{E - H_0 + i0^+}. \quad (4)$$

The key step is to numerically evaluate the Green functions, from which one obtains the scattering eigenstates [38]. Assuming a weak continuous wave incident laser, we calculate the second-order correlation function $g_2(t)$ [42] for an arbitrary interqubit separation.

Figure 2 shows $g_2(t)$ for both the transmitted and reflected fields when the probe laser is on resonance with

the qubit: $k = k_0$ ($k_0 \equiv \omega_0/c$). When the two qubits are colocated [9] ($L = 0$), $g_2(t)$ of the transmitted field shows strong initial bunching followed by antibunching, while $g_2(t)$ of the reflected field shows perfect antibunching at $t = 0$, $g_2(0) = 0$. This behavior is similar to that in the single qubit case [3, 8]. When the two qubits are spatially separated by $L = \pi/2k_0$, we observe quantum beats (oscillations). Since these beats occur in $g_2(t)$, they necessarily involve the nonlinearity of the qubits and do not occur for, *e.g.*, waveguide-coupled oscillators.

As one increases the separation L , one may expect from the well-known 3D result that the quantum beats disappear [43]. However, in our 1D system they do not: Figure 3 shows $g_2(t)$ for two cases, $k_0L = 25.5\pi$ and 100.5π , from which it is clear that the beats persist to long time. The 1D nature is key in producing strong quantum interference effects and so long-range qubit-qubit interactions.

Non-Markovian regime.—To interpret these exact numerical results, we compare them with the solution under the well-known Markov approximation. For small separations ($k_0L \leq \pi$), the system is Markovian [43]: the causal propagation time of photons between the two qubits can be neglected and so the qubits interact instantaneously. To understand quantum beats in this limit, we use a master equation for the density matrix ρ of the qubits in the Markov approximation. Integrating out the 1D bosonic degrees of freedom yields [34]

$$\begin{aligned} \frac{\partial \rho}{\partial t} &= \frac{i}{\hbar} [\rho, H_c] - \sum_{i,j=1,2} \frac{\Gamma_{ij}}{2} (\rho \sigma_i^+ \sigma_j^- + \sigma_i^+ \sigma_j^- \rho - 2\sigma_i^- \rho \sigma_j^+), \\ H_c &= \hbar\omega_0 \sum_{i=1,2} \sigma_i^+ \sigma_i^- + \hbar\Omega_{12}(\sigma_1^+ \sigma_2^- + \sigma_2^+ \sigma_1^-), \end{aligned} \quad (5)$$

where $\Gamma_{ii} \equiv \Gamma + \Gamma'$ while $\Gamma_{12} \equiv \Gamma \cos(\omega_0 L/c)$ and $\Omega_{12} \equiv (\Gamma/2) \sin(\omega_0 L/c)$ are the vacuum-mediated spontaneous and coherent couplings, respectively. Transforming to symmetric and antisymmetric states $|S, A\rangle = (|g_1 e_2\rangle \pm |e_1 g_2\rangle)/\sqrt{2}$ gives a more transparent form:

$$\begin{aligned} \frac{\partial \rho}{\partial t} &= \frac{i}{\hbar} [\rho, H_c] - \sum_{\beta=S,A} \frac{\Gamma_\beta}{2} (\rho \sigma_\beta^+ \sigma_\beta^- + \sigma_\beta^+ \sigma_\beta^- \rho - 2\sigma_\beta^- \rho \sigma_\beta^+), \\ H_c &= \sum_{\beta=S,A} \hbar\omega_\beta \sigma_\beta^+ \sigma_\beta^-, \end{aligned} \quad (6)$$

where $\sigma_{S,A}^\pm \equiv (\sigma_1^\pm \pm \sigma_2^\pm)/\sqrt{2}$, $\Gamma_{S,A} \equiv \Gamma + \Gamma' \pm \Gamma_{12}$, and $\omega_{S,A} \equiv \omega_0 \pm \Omega_{12}$. Note that $|S\rangle$ and $|A\rangle$ are decoupled from each other and have transition frequencies $\omega_{S,A}$ and decay rates $\Gamma_{S,A}$ which oscillate as a function of L . When $L = 0$, $\Gamma_S = 2\Gamma + \Gamma'$ and $\Gamma_A = \Gamma'$. $|S\rangle$ is in the superradiant state, while $|A\rangle$ is subradiant. The waveguide couples only to the superradiant state and so the photon-photon correlation mimics that for a single-qubit. However, when $k_0L = \pi/2$, $\Gamma_S = \Gamma_A = \Gamma + \Gamma'$, $\omega_{S,A} = \omega_0 \pm \Gamma/2$, and the waveguide couples to both $|S\rangle$ and $|A\rangle$. The quantum interference between the transitions $|S\rangle \rightarrow |g_1 g_2\rangle$ and $|A\rangle \rightarrow |g_1 g_2\rangle$ gives rise to quantum beats at frequency $\omega_S - \omega_A = \Gamma$, as shown in Fig. 2.

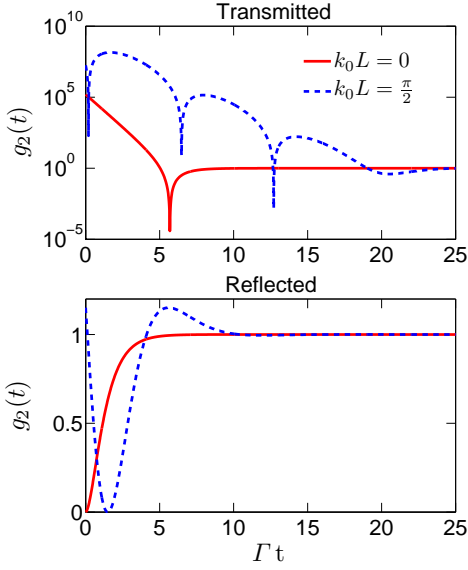


FIG. 2. Quantum beats in the Markovian regime. The second-order photon-photon correlation function of both the transmitted (top) and reflected (bottom) fields as a function of t for $k_0L = 0$ (solid line) and $k_0L = \pi/2$ (dashed line). The incident weak coherent state is on resonance with the qubits: $k = k_0 = \omega_0/c$. (Parameters: $\omega_0 = 100\Gamma$ and $\Gamma' = 0.1\Gamma$.)

As one increases the separation L and goes beyond the Markovian regime, Eq. (5) is not a valid description of the system because the causal propagation time of photons (or retardation effect) has to be included. Comparing the results in Figs. 2 and 3, we see that quantum beats are *more* visible in the non-Markovian regime in both the transmitted and reflected fields and persist to a much longer time scale, especially for the case $k_0L = 100.5\pi$.

To better understand the persistent quantum beats, we extract the transition frequencies and decay rates of the two qubit system beyond the Markovian regime. This is achieved by analyzing the poles of the Green function [38] defined in Eq. (4); they are given by

$$F(\omega) = \left[\omega - \omega_0 + \frac{i(\Gamma + \Gamma')}{2} \right]^2 + \frac{\Gamma^2}{4} e^{2i\omega L/c} = 0. \quad (7)$$

In the Markovian regime, one can safely replace ω by ω_0 in the exponent, given that $\omega_0 \gg \Gamma$ and $L \ll c\Gamma^{-1}$. Eq. (7) then yields $\omega_{\pm} = \omega_0 - i(\Gamma + \Gamma')/2 \pm i\Gamma e^{i\omega_0 L/c}/2$. The real and imaginary parts of ω_{\pm} correspond to the transition frequencies and decay rates, which are nothing but $\omega_{S,A}$ and $-\Gamma_{S,A}/2$ obtained using the Markov approximation [Eq. (6)]. Beyond this Markovian regime, we solve Eq. (7) iteratively by gradually increasing L .

Figure 4 shows that both $\omega_{S,A}$ and $\Gamma_{S,A}$ deviate significantly from their Markovian values as k_0L becomes large [Figs. 4(c) and 4(d)]. The expanded detail plots, Figs. 4(a) and 4(e), show that the Markov approximation works well for $k_0L \in [0, 5\pi]$. At large k_0L , however, *both* the symmetric and antisymmetric states become subra-

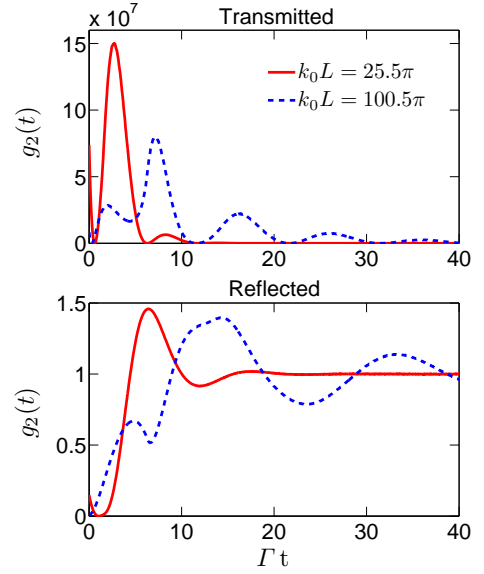


FIG. 3. Persistent quantum beats in the non-Markovian regime. The second-order correlation function of both the transmitted (top) and reflected (bottom) fields is plotted as a function of t for $k_0L = 25.5\pi$ (solid line) and 100.5π (dashed line). We set the incident coherent state on resonance with the qubits ($k = k_0$), $\omega_0 = 100\Gamma$ and $\Gamma' = 0.1\Gamma$.

diant [$\Gamma_{S,A} \ll \Gamma$, Fig. 4(f)]. This suppression of decay comes about in the following way: after the initial excitation of and emission from the first qubit, it can be re-excited by the pulse reflected from the second qubit. From the excitation probability of the first qubit through many emission-reexcitation cycles, an effective qubit life time can be defined: it is greatly lengthened by the causal propagation of photons between the two qubits. $\Gamma_{S,A}$ characterize the average long time decay quantitatively.

The nonlinear equation Eq. (7) gives rise, of course, to infinitely many poles for $L > 0$. These poles represent collective states of two spatially separated qubits with vacuum-mediated interactions. They are eigenmodes of the density matrix of the two qubits. The “two-pole” approximation of retaining only the symmetric and antisymmetric states is a good approximation because $(\omega_{S,A} - \omega_0, \Gamma_{S,A})$ are the two poles closest to the origin $(0, 0)$. Within the parameter range we consider, all other collective states are far detuned from ω_0 and hence barely populated [38]. In addition, $|S\rangle$ and $|A\rangle$ have much smaller decay rates than all the other collective states. Therefore, these two slowly decaying states dominate the long-time dynamics and quantum interference between their spontaneous emissions is the physical origin of the persistent quantum beats observed in Fig. 3.

Qubit-qubit entanglement.—With the two-pole approximation, we study qubit-qubit entanglement using the master equation Eq. (6) with $\omega_{S,A}$ and $\Gamma_{S,A}$ replaced by the renormalized values obtained from Eq. (7). We focus on the steady state case by including a continu-

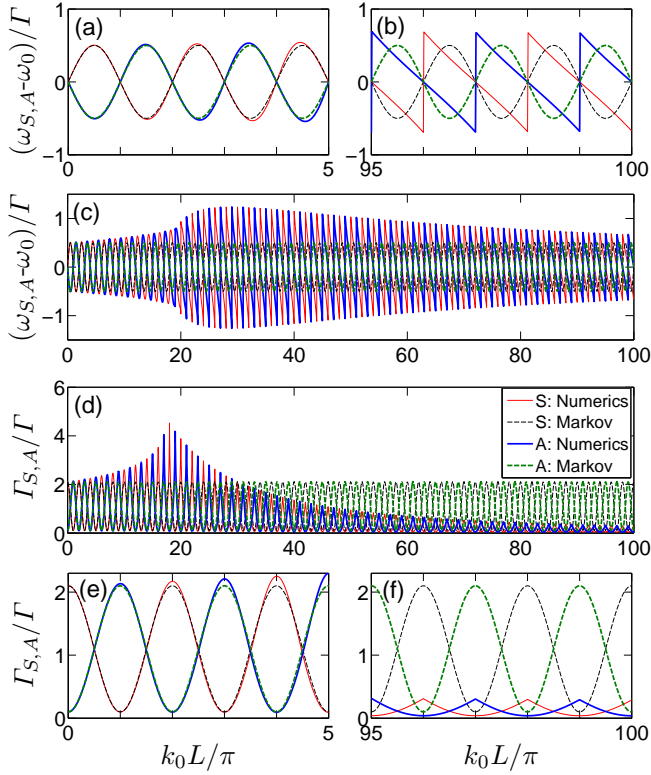


FIG. 4. Renormalized transition frequencies and decay rates of the symmetric (S) and antisymmetric (A) states. Panels (a)-(c) show the transition frequencies ω_S (thin solid line) and ω_A (thick solid line) obtained numerically from Eq. (7) together with ω_S (thin dashed line) and ω_A (thick dashed line) given by the Markov approximation. Panels (d)-(f) similarly show the decay rates Γ_S and Γ_A obtained both numerically and in the Markov approximation. ($\omega_0 = 100\Gamma$ and $\Gamma' = 0.1\Gamma$.)

ous weak driving laser on resonance with the first qubit: $H_L = \hbar\Omega_1(\sigma_1^+ + \sigma_1^-)$ [27, 28]. The entanglement is characterized by the concurrence [44]; Figure 5 shows its steady state value for the Rabi frequency $\Omega_1 = 0.1\Gamma$. For small separation [Fig. 5(a)], the concurrence agrees with that obtained using the Markov approximation [27]: C reaches its maximum when the maximally-entangled two-qubit subradiant state (either $|S\rangle$ or $|A\rangle$) has a minimal decay rate and is well populated [28]. Between two peaks, C vanishes because the symmetric and antisymmetric states are now barely populated and the usual decay rate, $\Gamma + \Gamma' \gg \Omega_1$, holds [45].

In contrast, Fig. 5(b) shows that the Markovian predictions break down: we observe enhanced entanglement for an arbitrary interqubit separation. Such enhancement is due to non-Markovian processes: both $|S\rangle$ and $|A\rangle$ become subradiant (Fig. 4) with decay rates much smaller than Γ and hence are well populated [38]. Thus, long-range entanglement is possible due to non-Markovian processes, making 1D waveguide-QED systems promising candidates for scalable quantum networking.

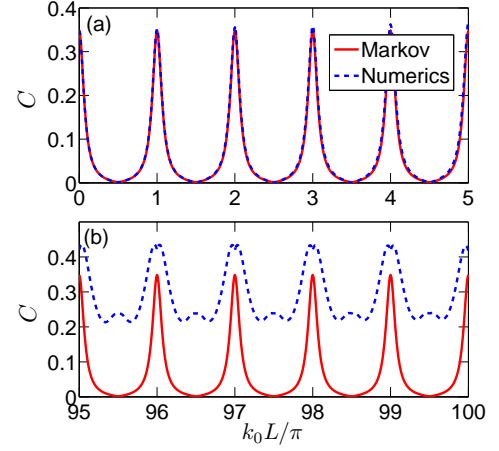


FIG. 5. Long-distance qubit-qubit entanglement. The steady state concurrence is plotted as a function of $k_0 L$ for (a) $0 \leq k_0 L \leq 5\pi$, and (b) $95\pi \leq k_0 L \leq 100\pi$. The Rabi frequencies are $\Omega_1 = 0.1\Gamma$, $\Omega_2 = 0$. The driving laser is on resonance with the qubits. ($\omega_0 = 100\Gamma$ and $\Gamma' = 0.1\Gamma$.)

Discussion of loss.—Accessing the non-Markovian regime requires a large (effective) distance between the qubits and hence low loss in the waveguide. Here, we have included the loss of the qubit by using an effective Purcell factor of 10 (*i.e.* $\sim 10\%$ loss). Because waveguide loss has the same effect on system performance as qubit loss (both lead to photon leakage), we expect that the observed persistent quantum beats and long-distance entanglement are robust against waveguide loss on this same level, namely $\sim 10\%$. While some waveguides in current experimental systems are very lossy (such as plasmonic nanowires [15]), we can circumvent this difficulty by using a hybrid nanofiber system as discussed in the Supplementary Material [38]. One example is an integrated fiber-plasmonic system [3]: the optical fiber is coupled to two tapered plasmonic nanowires which interact with local qubits (*e.g.* quantum dots). Another example is an integrated nanofiber-trapped atomic ensemble [46, 47]: an optical fiber is tapered into a nanofiber in two regions where atomic ensembles are trapped by the evanescent field surrounding the nanofibers. In both of these examples, the long waveguide connecting the two qubits is a high quality optical fiber in which the loss is very small over a length of the order of 100 wavelengths.

We thank D. J. Gauthier for valuable discussions. This work was supported by U.S. NSF Grant No. PHY-10-68698. H.Z. is supported by a John T. Chambers Fellowship from the Fitzpatrick Institute for Photonics at Duke University. We thank the Fondation Nanosciences of Grenoble, France, for its hospitality during completion of this work.

* hz33@duke.edu

† baranger@phy.duke.edu

- [1] H. J. Kimble, *Nature*, **453**, 1023 (2008).
- [2] D. E. Chang, A. S. Sørensen, P. R. Hemmer, and M. D. Lukin, *Phys. Rev. Lett.*, **97**, 053002 (2006).
- [3] D. E. Chang, A. S. Sørensen, E. A. Demler, and M. D. Lukin, *Nature Phys.*, **3**, 807 (2007).
- [4] J.-T. Shen and S. Fan, *Phys. Rev. Lett.*, **98**, 153003 (2007); *Phys. Rev. A*, **76**, 062709 (2007).
- [5] L. Zhou, Z. R. Gong, Y.-X. Liu, C. P. Sun, and F. Nori, *Phys. Rev. Lett.*, **101**, 100501 (2008).
- [6] P. Longo, P. Schmitteckert, and K. Busch, *Phys. Rev. Lett.*, **104**, 023602 (2010).
- [7] D. Witthaut and A. S. Sørensen, *New J. Phys.*, **12**, 043052 (2010).
- [8] H. Zheng, D. J. Gauthier, and H. U. Baranger, *Phys. Rev. A*, **82**, 063816 (2010).
- [9] E. Rephaeli, S. E. Kocabas, and S. Fan, *Phys. Rev. A*, **84**, 063832 (2011).
- [10] D. Roy, *Phys. Rev. Lett.*, **106**, 053601 (2011).
- [11] D. Roy, *Phys. Rev. A*, **83**, 043823 (2011).
- [12] P. Kolchin, R. F. Oulton, and X. Zhang, *Phys. Rev. Lett.*, **106**, 113601 (2011).
- [13] H. Zheng, D. J. Gauthier, and H. U. Baranger, *Phys. Rev. Lett.*, **107**, 223601 (2011); *Phys. Rev. A*, **85**, 043832 (2012).
- [14] E. Rephaeli and S. Fan, *Phys. Rev. Lett.*, **108**, 143602 (2012).
- [15] A. V. Akimov, A. Mukherjee, C. L. Yu, D. E. Chang, A. S. Zibrov, P. R. Hemmer, H. Park, and M. D. Lukin, *Nature*, **450**, 402 (2007).
- [16] M. Bajcsy, S. Hofferberth, V. Balic, T. Peyronel, M. Hafezi, A. S. Zibrov, V. Vuletic, and M. D. Lukin, *Phys. Rev. Lett.*, **102**, 203902 (2009).
- [17] T. M. Babinec, B. J. M. Hausmann, M. Khan, Y. Zhang, J. R. Maze, P. R. Hemmer, and M. Lončar, *Nature Nanotech.*, **5**, 195 (2010).
- [18] J. Claudon, J. Bleuse, N. S. Malik, M. Bazin, P. Jaffrennou, N. Gregersen, C. Sauvan, P. Lalanne, and J.-M. Gérard, *Nat. Photon.*, **4**, 174 (2010).
- [19] O. Astafiev, A. M. Zagoskin, A. A. Abdumalikov, Y. A. Pashkin, T. Yamamoto, K. Inomata, Y. Nakamura, and J. S. Tsai, *Science*, **327**, 840 (2010).
- [20] O. V. Astafiev, A. A. Abdumalikov, A. M. Zagoskin, Y. A. Pashkin, Y. Nakamura, and J. S. Tsai, *Phys. Rev. Lett.*, **104**, 183603 (2010).
- [21] J. Bleuse, J. Claudon, M. Creasey, N. S. Malik, J.-M. Gérard, I. Maksymov, J.-P. Hugonin, and P. Lalanne, *Phys. Rev. Lett.*, **106**, 103601 (2011).
- [22] I.-C. Hoi, C. M. Wilson, G. Johansson, T. Palomaki, B. Peropadre, and P. Delsing, *Phys. Rev. Lett.*, **107**, 073601 (2011).
- [23] A. Laucht, S. Pütz, T. Günthner, N. Hauke, R. Saive, S. Frédérick, M. Bichler, M.-C. Amann, A. W. Holleitner, M. Kaniber, and J. J. Finley, *Phys. Rev. X*, **2**, 011014 (2012).
- [24] I.-C. Hoi, T. Palomaki, J. Lindkvist, G. Johansson, P. Delsing, and C. M. Wilson, *Phys. Rev. Lett.*, **108**, 263601 (2012).
- [25] D. Dzsojtan, A. S. Sørensen, and M. Fleischhauer, *Phys. Rev. B*, **82**, 075427 (2010).
- [26] D. Dzsojtan, J. Kästel, and M. Fleischhauer, *Phys. Rev. B*, **84**, 075419 (2011).
- [27] A. Gonzalez-Tudela, D. Martin-Cano, E. Moreno, L. Martin-Moreno, C. Tejedor, and F. J. Garcia-Vidal, *Phys. Rev. Lett.*, **106**, 020501 (2011).
- [28] D. Martin-Cano, A. Gonzalez-Tudela, L. Martin-Moreno, F. J. Garcia-Vidal, C. Tejedor, and E. Moreno, *Phys. Rev. B*, **84**, 235306 (2011).
- [29] J. P. Paz and A. J. Roncaglia, *Phys. Rev. Lett.*, **100**, 220401 (2008).
- [30] T. Zell, F. Queisser, and R. Klesse, *Phys. Rev. Lett.*, **102**, 160501 (2009).
- [31] H.-T. Tan, W.-M. Zhang, and G.-x. Li, *Phys. Rev. A*, **83**, 062310 (2011).
- [32] A. Wolf, G. D. Chiara, E. Kajari, E. Lutz, and G. Morigi, *Europhys. Lett.*, **95**, 60008 (2011).
- [33] J. Majer, J. M. Chow, J. M. Gambetta, J. Koch, B. R. Johnson, J. A. Schreier, L. Frunzio, D. I. Schuster, A. A. Houck, A. Wallraff, A. Blais, M. H. Devoret, S. M. Girvin, and R. J. Schoelkopf, *Nature*, **449**, 443 (2007).
- [34] Z. Ficek and R. Tanas, *Phys. Rep.*, **372**, 369 (2002).
- [35] S. Das, G. S. Agarwal, and M. O. Scully, *Phys. Rev. Lett.*, **101**, 153601 (2008).
- [36] Note that we adopt the rotating wave approximation (RWA) at the level of Hamiltonian. As pointed out in [48], within the RWA causality in photon propagation is preserved by extending the frequency integrals to minus infinity. We carry out this scheme in all of our numerical calculations.
- [37] H. J. Carmichael, *An Open Systems Approach to Quantum Optics (Lecture Notes in Physics)* (Springer, Berlin, 1993).
- [38] See Supplementary Materials for details.
- [39] L.-M. Duan and H. J. Kimble, *Phys. Rev. Lett.*, **92**, 127902 (2004).
- [40] J. J. Sakurai, *Modern Quantum Mechanics* (Addison-Wesley, Reading, MA, 1994).
- [41] A. Dhar, D. Sen, and D. Roy, *Phys. Rev. Lett.*, **101**, 066805 (2008).
- [42] R. Loudon, *The Quantum Theory of Light*, 3rd ed. (Oxford University Press, New York, 2003).
- [43] Z. Ficek and B. C. Sanders, *Phys. Rev. A*, **41**, 359 (1990).
- [44] W. K. Wootters, *Phys. Rev. Lett.*, **80**, 2245 (1998).
- [45] The population of an excited state with detuning Δ , decay rate Γ , and Rabi frequency Ω is given by $1/[2 + (\Delta/\Omega)^2 + (\Gamma/2\Omega)^2]$.
- [46] E. Vetsch, D. Reitz, G. Sagué, R. Schmidt, S. T. Dawkins, and A. Rauschenbeutel, *Phys. Rev. Lett.*, **104**, 203603 (2010).
- [47] A. Goban, K. S. Choi, D. J. Alton, D. Ding, C. Lacroûte, M. Pototschnig, T. Thiele, N. P. Stern, and H. J. Kimble, *Phys. Rev. Lett.*, **109**, 033603 (2012).
- [48] P. W. Milonni, D. F. V. James, and H. Fearn, *Phys. Rev. A*, **52**, 1525 (1995).
- [49] O. Benson, *Nature*, **480**, 193 (2011).
- [50] T. Tobias, J. Thompson, J. Feist, C. Yu, A. Akimov, D. Chang, A. Zibrov, V. Vuletic, H. Park, and M. Lukin, "A nanoscale quantum interface for single atoms," Abstract APS 2012 March Meeting (2012).
- [51] R. F. Oulton, V. J. Sorger, D. A. Genov, D. F. P. Pile, and X. Zhang, *Nat. Photon.*, **2**, 496 (2008).
- [52] J. Feist, S. K. Saikin, M. H. Reid, A. Aspuru-Guzik, and M. D. Lukin, "Plasmonic nanotips for spectroscopy with nanometer-scale resolution," Abstract APS 2012 March

Meeting (2012).

[53] C.-L. Zou, F.-W. Sun, C.-H. Dong, Y.-F. Xiao, X.-F. Ren, X.-D. C. Liu Lv, J.-M. Cui, Z.-F. Han, , and G.-C.

Guo, IEEE Photon. Tech. Letts., **24**, 1041 (2012).

[54] J. T. Shen and S. Fan, Phys. Rev. B, **75**, 035320 (2007).

Supplementary Material for “Persistent Quantum Beats and Long-Distance Entanglement from Waveguide-Mediated Interactions”

In this Supplementary Material we address the following topics: calculation of single-photon scattering eigenstates, our numerical Green function method, the two pole approximation, and possible low-loss systems for long-distance entanglement.

Single-Photon Scattering Eigenstates

A general single-photon scattering eigenstate of the system described by Eq. (1) in the main text reads

$$|\phi_1\rangle = \int dx \left[\phi_R(x) a_R^\dagger(x) + \phi_L(x) a_L^\dagger(x) + e_1 \sigma_1^+ + e_2 \sigma_2^+ \right] |0, g_1 g_2\rangle, \quad (\text{S1})$$

where $|0, g_1 g_2\rangle$ is the zero photon state with both qubits in the ground state. The Schrödinger equation $H|\phi_1\rangle = E|\phi_1\rangle$ gives

$$\begin{aligned} \left[-i\hbar c \frac{d}{dx} - E \right] \phi_R(x) + \hbar V_1 \delta(x - \ell_1) e_1 + \hbar V_2 \delta(x - \ell_2) e_2 &= 0, \\ \left[i\hbar c \frac{d}{dx} - E \right] \phi_L(x) + \hbar V_1 \delta(x - \ell_1) e_1 + \hbar V_2 \delta(x - \ell_2) e_2 &= 0, \\ (\hbar \omega_1 - i\Gamma'_1/2 - E) e_1 + \hbar V_1 [\phi_R(\ell_1) + \phi_L(\ell_1)] &= 0, \\ (\hbar \omega_2 - i\Gamma'_2/2 - E) e_2 + \hbar V_2 [\phi_R(\ell_2) + \phi_L(\ell_2)] &= 0. \end{aligned} \quad (\text{S2})$$

Assuming an incident right-going photon of wave vector $k = E/c$, the wavefunction takes the following form

$$\begin{aligned} \phi_R(x) &= \frac{e^{ikx}}{\sqrt{2\pi}} [\theta(\ell_1 - x) + t_{12}\theta(x - \ell_1)\theta(\ell_2 - x) + t_k\theta(x - \ell_2)], \\ \phi_L(x) &= \frac{e^{-ikx}}{\sqrt{2\pi}} [r_k\theta(\ell_1 - x) + r_{12}\theta(x - \ell_1)\theta(\ell_2 - x)], \end{aligned} \quad (\text{S3})$$

where $\theta(x)$ is the step function. Setting $\phi_{R,L}(\ell_{1,2}) = [\phi_{R,L}(\ell_{1,2}^+) + \phi_{R,L}(\ell_{1,2}^-)]/2$ and plugging Eq. (S3) into (S2), we obtain the following solution

$$\begin{aligned} t_{12} &= \frac{(ck - \omega_1 + i\Gamma'_1/2)(ck - \omega_2 + i\Gamma'_2/2 + i\Gamma_2/2)}{(ck - \omega_1 + i\Gamma'_1/2 + i\Gamma_1/2)(ck - \omega_2 + i\Gamma'_2/2 + i\Gamma_2/2) + \Gamma_1\Gamma_2 e^{2ikL}/4}, \\ r_{12} &= \frac{-i\Gamma_2(ck - \omega_1 + i\Gamma'_1/2)e^{2ik\ell_2}/2}{(ck - \omega_1 + i\Gamma'_1/2 + i\Gamma_1/2)(ck - \omega_2 + i\Gamma'_2/2 + i\Gamma_2/2) + \Gamma_1\Gamma_2 e^{2ikL}/4}, \\ t_k &= \frac{(ck - \omega_1 + i\Gamma'_1/2)(ck - \omega_2 + i\Gamma'_2/2)}{(ck - \omega_1 + i\Gamma'_1/2 + i\Gamma_1/2)(ck - \omega_2 + i\Gamma'_2/2 + i\Gamma_2/2) + \Gamma_1\Gamma_2 e^{2ikL}/4}, \\ r_k &= \frac{-i\Gamma_2(ck - \omega_1 + i\Gamma'_1/2 - i\Gamma_1/2)e^{2ik\ell_2}/2 - i\Gamma_1(ck - \omega_2 + i\Gamma'_2/2 + i\Gamma_2/2)e^{2ik\ell_1}/2}{(ck - \omega_1 + i\Gamma'_1/2 + i\Gamma_1/2)(ck - \omega_2 + i\Gamma'_2/2 + i\Gamma_2/2) + \Gamma_1\Gamma_2 e^{2ikL}/4}, \\ e_1 &= \left(ic\sqrt{\frac{2}{\Gamma_1}} \right) \frac{e^{ik\ell_1}}{\sqrt{2\pi}} (t_{12} - 1), \quad e_2 = \left(ic\sqrt{\frac{2}{\Gamma_2}} \right) \frac{e^{ik\ell_2}}{\sqrt{2\pi}} (t_k - t_{12}). \end{aligned} \quad (\text{S4})$$

In the case of two identical qubits, t_k reduces to the expression given in Eq. (2) in the main text.

Similarly, we can solve for the single-photon scattering eigenstate for an incident right-going photon of wave vector $k = E/c$. We represent the wavefunction with an incident right-going and left-going photon by $|\phi_1(k)\rangle_R$ and $|\phi_1(k)\rangle_L$, respectively.

Numerical Green Function Method

With the Lippmann-Schwinger equation shown in Eq. (4) of the main text, we can solve for the full interacting solution. The non-interacting eigenstates are simply products of single-photon states.

$$\begin{aligned} |\phi_n(k_1, \dots, k_n)\rangle_{\alpha_1, \dots, \alpha_n} &= |\phi_1(k_1)\rangle_{\alpha_1} |\phi_1(k_2)\rangle_{\alpha_2} \cdots |\phi_1(k_n)\rangle_{\alpha_n}, \quad \alpha_j = R, L, j = 1-n, \\ H_0 |\phi_n(k_1, \dots, k_n)\rangle_{\alpha_1, \dots, \alpha_n} &= c(k_1 + \dots + k_n) |\phi_n(k_1, \dots, k_n)\rangle_{\alpha_1, \dots, \alpha_n}. \end{aligned} \quad (S5)$$

For simplicity, we will focus on the two-particle solution from now on. Extending the formalism to the many-particle solution is straightforward. The two-particle identity in real-space can be written as

$$\begin{aligned} I_2 &= I_2^x \otimes |\emptyset\rangle\langle\emptyset| + I_1^x \otimes \sum_{i=1,2} |d_i\rangle\langle d_i| + I_0^x \otimes \sum_{i \leq j} |d_i d_j\rangle\langle d_i d_j|, \\ I_n^x &= \sum_{\alpha_1 \cdots \alpha_n = R, L} \int dx_1 \cdots dx_n |x_1 \cdots x_n\rangle_{\alpha_1 \cdots \alpha_n} \langle x_1 \cdots x_n|, \end{aligned} \quad (S6)$$

where $|\emptyset\rangle$ is the ground state of the two qubits (bosonic sites), $|d_i\rangle = d_i^\dagger |\emptyset\rangle$, $|d_i d_i\rangle = \frac{(d_i^\dagger)^2}{\sqrt{2}} |\emptyset\rangle$ and $|d_1 d_2\rangle = d_1^\dagger d_2^\dagger |\emptyset\rangle$. Inserting the above identity into Eq. (4) in the main text, we obtain

$$\begin{aligned} |\psi_2(k_1, k_2)\rangle_{\alpha_1, \alpha_2} &= |\phi_2(k_1, k_2)\rangle_{\alpha_1, \alpha_2} + G^R(E) V I_2 |\psi_2(k_1, k_2)\rangle_{\alpha_1, \alpha_2} \\ &= |\phi_2(k_1, k_2)\rangle_{\alpha_1, \alpha_2} + U G^R(E) \sum_{i=1,2} |d_i d_i\rangle\langle d_i d_i| \psi_2(k_1, k_2)\rangle_{\alpha_1, \alpha_2}. \end{aligned} \quad (S7)$$

Projecting Eq. (S7) onto $\langle d_i d_i|$ yields

$$\begin{pmatrix} \langle d_1 d_1 | \psi_2(k_1, k_2) \rangle_{\alpha_1, \alpha_2} \\ \langle d_2 d_2 | \psi_2(k_1, k_2) \rangle_{\alpha_1, \alpha_2} \end{pmatrix} = \begin{pmatrix} \langle d_1 d_1 | \phi_2(k_1, k_2) \rangle_{\alpha_1, \alpha_2} \\ \langle d_2 d_2 | \phi_2(k_1, k_2) \rangle_{\alpha_1, \alpha_2} \end{pmatrix} + U \begin{bmatrix} G_{11} & G_{12} \\ G_{21} & G_{22} \end{bmatrix} \begin{pmatrix} \langle d_1 d_1 | \psi_2(k_1, k_2) \rangle_{\alpha_1, \alpha_2} \\ \langle d_2 d_2 | \psi_2(k_1, k_2) \rangle_{\alpha_1, \alpha_2} \end{pmatrix}, \quad (S8)$$

where we introduce the short-hand notation $G_{ij} = \langle d_i d_i | G^R(E) | d_j d_j \rangle$. Solving Eq. (S8) gives rise to

$$\begin{pmatrix} \langle d_1 d_1 | \psi_2(k_1, k_2) \rangle_{\alpha_1, \alpha_2} \\ \langle d_2 d_2 | \psi_2(k_1, k_2) \rangle_{\alpha_1, \alpha_2} \end{pmatrix} = \left(I - U \begin{bmatrix} G_{11} & G_{12} \\ G_{21} & G_{22} \end{bmatrix} \right)^{-1} \begin{pmatrix} \langle d_1 d_1 | \phi_2(k_1, k_2) \rangle_{\alpha_1, \alpha_2} \\ \langle d_2 d_2 | \phi_2(k_1, k_2) \rangle_{\alpha_1, \alpha_2} \end{pmatrix}. \quad (S9)$$

Projecting Eq. (S7) onto a two-photon basis state $\langle x_1 x_2|$ and taking the $U \rightarrow \infty$ limit, we obtain the full interacting two-photon solution

$$\begin{aligned} \langle x_1 x_2 | \psi_2(k_1, k_2) \rangle_{\alpha_1, \alpha_2} &= \langle x_1 x_2 | \phi_2(k_1, k_2) \rangle_{\alpha_1, \alpha_2} + U \begin{pmatrix} G_1(x_1, x_2) & G_2(x_1, x_2) \end{pmatrix} \begin{pmatrix} \langle d_1 d_1 | \psi_2(k_1, k_2) \rangle_{\alpha_1, \alpha_2} \\ \langle d_2 d_2 | \psi_2(k_1, k_2) \rangle_{\alpha_1, \alpha_2} \end{pmatrix} \\ &= \langle x_1 x_2 | \phi_2(k_1, k_2) \rangle_{\alpha_1, \alpha_2} - G_{xd} G_{dd}^{-1} \begin{pmatrix} \langle d_1 d_1 | \phi_2(k_1, k_2) \rangle_{\alpha_1, \alpha_2} \\ \langle d_2 d_2 | \phi_2(k_1, k_2) \rangle_{\alpha_1, \alpha_2} \end{pmatrix}, \end{aligned} \quad (S10)$$

where $G_i(x_1, x_2) = \langle x_1 x_2 | G^R(E) | d_i d_i \rangle$ and

$$\begin{aligned} G_{xd} &\equiv \begin{pmatrix} G_1(x_1, x_2) & G_2(x_1, x_2) \end{pmatrix}, \\ G_{dd} &\equiv \begin{bmatrix} G_{11} & G_{12} \\ G_{21} & G_{22} \end{bmatrix}. \end{aligned} \quad (S11)$$

Hence, the remaining task is to calculate all the Green functions in Eq. (S10). This can be done using the two-photon non-interacting scattering eigenstates, from which we can construct a two-particle identity in momentum space

$$I_2' = \sum_{\alpha_1, \alpha_2 = R, L} \int dk_1 dk_2 |\phi_2(k_1, k_2)\rangle_{\alpha_1, \alpha_2} \langle \phi_2(k_1, k_2)|. \quad (S12)$$

Using Eq. (S5), the Green functions can be evaluated as

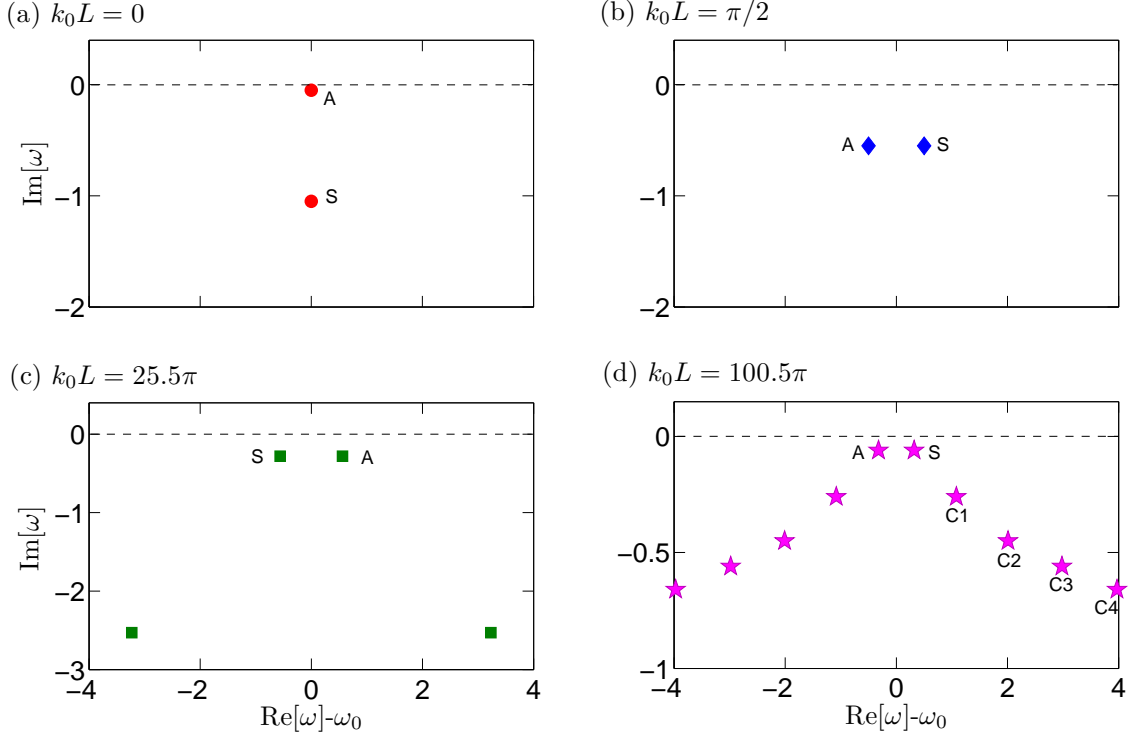


FIG. S1. The poles of the Green functions for (a) $k_0L = 0$, (b) $k_0L = \frac{\pi}{2}$, (c) $k_0L = 25.5\pi$, and (d) $k_0L = 100.5\pi$. Both the real and imaginary parts of the poles are in units of Γ . We show all the poles with real part within $[\omega_0 - 4\Gamma, \omega_0 + 4\Gamma]$. The poles corresponding to the $|S\rangle$ and $|A\rangle$ states are labeled as S and A , respectively. In case (d), there are four additional poles ($C1$ - $C4$) within the plotted range.

$$\begin{aligned}
 G_{ij} &= \langle d_i d_i | G^R(E) I'_2 | d_j d_j \rangle \\
 &= \sum_{\alpha_1, \alpha_2=R,L} \int dk_1 dk_2 \frac{1}{E - ck_1 - ck_2 + i0^+} \langle d_i d_i | \phi_2(k_1, k_2) \rangle_{\alpha_1, \alpha_2} \langle \phi_2(k_1, k_2) | d_j d_j \rangle, \\
 G_i(x_1, x_2) &= \langle x_1 x_2 | G^R(E) I'_2 | d_i d_i \rangle \\
 &= \sum_{\alpha_1, \alpha_2=R,L} \int dk_1 dk_2 \frac{1}{E - ck_1 - ck_2 + i0^+} \langle x_1 x_2 | \phi_2(k_1, k_2) \rangle_{\alpha_1, \alpha_2} \langle \phi_2(k_1, k_2) | d_i d_i \rangle.
 \end{aligned} \tag{S13}$$

Doing the integrals numerically gives the full interacting two-particle solution. Again, following the same program, it is straightforward to extend the formalism to the three- or more photon solution with two or more qubits coupled to the waveguide.

Two-Pole Approximation

In this section, we will show the validity of the ‘two-pole’ approximation in the parameter regime we consider. Assuming two identical qubits, the poles of the Green functions in Eq. (S10) are given by

$$F(\omega) = \left[\omega - \omega_0 + \frac{i(\Gamma + \Gamma')}{2} \right]^2 + \frac{\Gamma^2}{4} e^{2i\omega L/c} = 0. \tag{S14}$$

Figure S1 plots the poles computed numerically in four different cases. For small L , Figs. S1(a) and S1(b) show that there are only two poles corresponding to $|S\rangle$ and $|A\rangle$ states within a large range of frequency. At large L , however, both the symmetric and antisymmetric states become subradiant [$\Gamma_{S,A} \ll \Gamma$]. This suppression of decay comes about in the following way: after the initial excitation of and emission from the first qubit, it can be reexcited by the pulse reflected from the second qubit. From the excitation probability of the first qubit through many emission-reexcitation cycles, an effective qubit life time can be defined: it is greatly lengthened by the causal propagation of photons between the two qubits. $\Gamma_{S,A}$ characterize the average long time decay quantitatively. Furthermore, as L increases, there are

additional poles as shown in Figs.S1(c) and S1(d), corresponding to collective states generated in non-Markovian processes. For $L \gg c\Gamma^{-1}$, the two-pole approximation breaks down as the additional poles of collective states become close enough to $|S\rangle$ and $|A\rangle$ states.

Here, we want to analyze the case $k_0L = 100.5\pi$ [Fig. S1(d)], where $L \sim c\Gamma^{-1}$ and the two-pole approximation is still valid as we will show below. With a driving laser on resonance with the qubits and a Rabi frequency Ω , the probability to excite a state $|y\rangle$ (ω_y, Γ_y) is

$$P_y = \frac{1}{2 + \left(\frac{\omega_y - \omega_0}{\Omega}\right)^2 + \left(\frac{\Gamma_y}{2\Omega}\right)^2}. \quad (\text{S15})$$

Using this formula, we can calculate the probability of exciting the states corresponding to S ($\omega_0 + 0.32\Gamma, 0.12\Gamma$), A ($\omega_0 - 0.32\Gamma, 0.12\Gamma$), $C1$ ($\omega_0 + 1.08\Gamma, 0.52\Gamma$), $C2$ ($\omega_0 + 2.01\Gamma, 0.90\Gamma$), $C3$ ($\omega_0 + 2.98\Gamma, 1.12\Gamma$) and $C4$ ($\omega_0 + 3.97\Gamma, 1.32\Gamma$). In the limit of weak driving laser, $\Omega \rightarrow 0$, we have

$$\begin{aligned} P_{C1} &= 8.6\%P_S, \\ P_{C2} &= 2.5\%P_S, \\ P_{C3} &= 1.1\%P_S, \\ P_{C4} &= 0.7\%P_S. \end{aligned} \quad (\text{S16})$$

Hence, compared to states $C1$ - $C4$, S and A states are well populated and dominate the qubit-qubit interactions for the parameter regime considered in the main text.

Possible Low-Loss Systems for Long-Distance Entanglement

In this section, we discuss the issue of waveguide loss and propose several low-loss systems to overcome this difficulty. As discussed in the main text, waveguide loss has to be limited to the same level as qubit loss. However, some waveguides in current experiments, *e.g.* plasmonic nanowires, are too lossy to meet this criteria. We propose to use either a hybrid optical fiber systems or slow-light superconducting systems. In the first case, low-loss optical fibers are used to transmit light over a long distance. The transmission length we are considering is of order 100 wavelengths, thus of order 100 microns for typical quantum dots or atoms. Loss over such a distance in state of the art fiber is very small: taking a 4dB/km fiber, the loss will be on the order of 1 ppm. In the second case, the actual transmission length is very short, but due to the reduced speed of light one can still reach the non-Markovian regime. Below are three plausible experimental settings: (a) and (b) belong to the first case and (c) illustrates the second case.

(a) Hybrid Fiber-Plasmonic Waveguide-QED System

Figure S2(a) shows an integrated fiber-plasmonic waveguide-QED system. The idea of hybrid plasmonic systems was first proposed by Chang et al. [3]. Since then, there has been extensive experimental [49, 50], and theoretical [51–53] work along this line. In the schematic, the optical fiber is coupled to two tapered plasmonic nanowires. Due to the subwavelength confinement [3], the plasmonic field in the nanowires couples strongly to the local qubits, *e.g.* quantum dots [15]. Coupling the nanowires to a dielectric waveguide ensures that the quantum state can be transmitted over long distance without being dissipated in the nanowires.

(b) Integrated Nanofiber-Trapped Atomic Ensemble System

In the second example, a long optical fiber is tapered into a narrow nanofiber in two regions. Then, two atomic ensembles are trapped by the evanescent field surrounding the nanofibers. Strong coupling is achieved between the propagating photons in the nanofiber and the atomic ensembles [46]. Such a setting is a clear extension of the experimental systems demonstrated by several groups [46, 47].

(c) Slow-light Superconducting Waveguide-QED System

In the third example, a 1D open superconducting transmission line is coupled to two superconducting qubits. It has been experimentally demonstrated that this system is deep in the strong coupling regime [22]. However, the typical length of the transmission line is on the order of the wavelength of propagating microwave photons. Hence, the separation of the two qubits is limited to the photon wavelength. To reach the non-Markovian regime, we can make the effective distance between the two qubits large by the slow-light scheme first proposed by Shen and Fan [54]. The idea is to couple the transmission line to an additional periodic array of unit cells made of two qubits. Flat photonic bands can be generated to slow down the microwave photons. While not true long-distance propagation, this could be an effective way to experimentally probe non-Markovian effects.

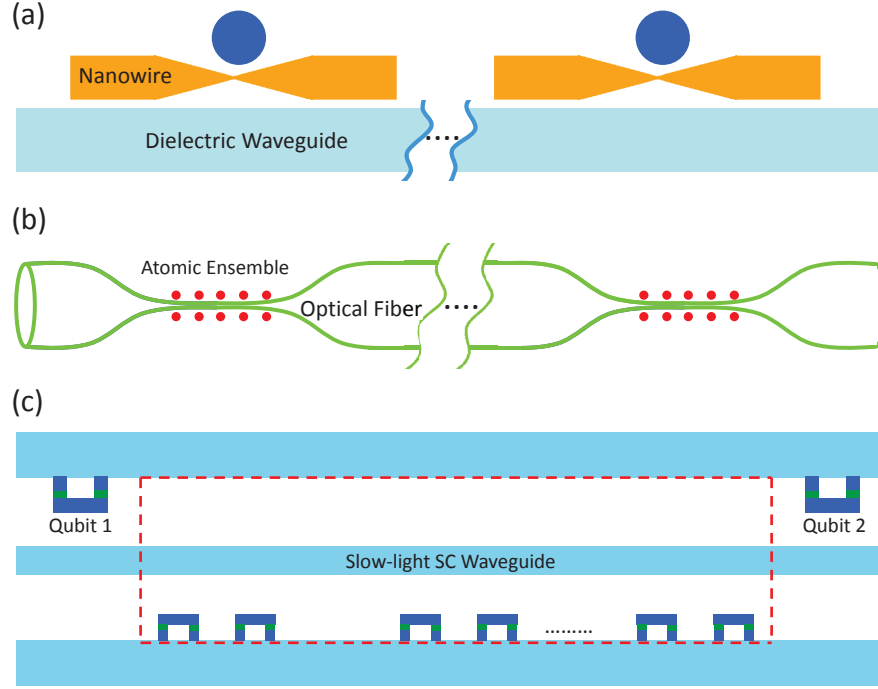


FIG. S2. Three possible setups for long-distance entanglement in waveguide-QED. (a) Hybrid plasmonic system. The dielectric waveguide (light blue) is phase-matched with the plasmonic nanowires (yellow) so that efficient plasmon transfer between them can be realized. The nanowires are strongly coupled to the quantum dots (blue) in the tapered regions. Note that the length of the dielectric waveguide between the nanowires can be very long (indicated by breaks). (b) Tapered nanofiber system. An optical fiber (green) is tapered into narrow nanofibers in two regions. Two atomic ensembles (red) are trapped by and strongly coupled to the nanofibers. (c) Slow-light superconducting system. Two superconducting qubits (blue) couple strongly to the slow-light superconducting waveguide (red dashed box).